Chemical Geology 345 (2013) 87–98

Contents lists available at SciVerse ScienceDirect

Chemical Geology

journal homepage: www.elsevier.com/locate/chemgeo

Age intercalibration of $^{40}Ar/^{39}Ar$ sanidine and chemically distinct U/Pb zircon populations from the Alder Creek Rhyolite Quaternary geochronology standard

Tiffany A. Rivera [a,*], Michael Storey [a], Mark D. Schmitz [b], James L. Crowley [b]

[a] Quaternary Dating Laboratory, Department of Environmental, Social and Spatial Change, Roskilde University, P.O. Box 260, 4000 Roskilde, Denmark
[b] Department of Geosciences, Boise State University, 1910 University Dr., Boise, ID 83725, USA

ARTICLE INFO

Article history:
Received 12 October 2012
Received in revised form 23 February 2013
Accepted 23 February 2013
Available online 5 March 2013

Editor: L. Reisberg

Keywords:
Geochronology
EARTHTIME
Quaternary
Intercalibration
Pleistocene
Cobb Mountain

ABSTRACT

We report results from a $^{40}Ar/^{39}Ar$ sanidine and CA-TIMS $^{238}U/^{206}Pb$ zircon dating study of eruption and crystal residence timescales of the Alder Creek Rhyolite (ACR), California, extruded during the Cobb Mountain normal-polarity subchron (C1r.2n). A $^{40}Ar/^{39}Ar$ ACR sanidine date of 1.1850 ± 0.0016 Ma (2σ external uncertainty), determined relative to the astronomically dated A1 tephra sanidine, is interpreted as the ACR eruption age. This age is supported by CA-TIMS U–Pb zircon dating, guided by LA-ICPMS trace element analyses, titanium-in-zircon (TiZR) thermometry, and cathodoluminescence (CL) imaging. Using these data, two compositionally distinct zircon populations were revealed. "Pre-ACR" Group B zircon exhibit oscillatory zoning, large positive Ce and negative Eu anomalies, high incompatible trace element contents, TiZR temperatures of 650 °C–750 °C, and Th/U disequilibrium corrected $^{238}U/^{206}Pb$ dates of 1.38–1.24 Ma. These crystals are interpreted as antecrysts inherited from earlier intrusives in the Geysers–Cobb Mountain magma source region. "ACR-related" Group A zircon, present as discrete grains and overgrowths on Group B zircon, display less intense CL with diffuse zoning, and have less pronounced positive Ce and negative Eu anomalies, lower incompatible trace element contents, higher TiZR temperatures that range up to 840 °C, and significantly younger dates. The youngest Group A dates yield a weighted mean of 1.1978 ± 0.0046 Ma (2σ, including systematic uncertainties) that is interpreted as the mean age of zircon crystallization prior to eruption. The 13 ± 5 ka offset between the $^{40}Ar/^{39}Ar$ and $^{238}U/^{206}Pb$ dates can be attributed to zircon magma residence time. Recognition of a young population of ACR zircon is consistent with the $^{40}Ar/^{39}Ar$ eruption age, which coincides with the astronomical age estimate for the Cobb Mountain subchron determined by correlating the oxygen isotope record of the giant piston core MD972143 to the $La93_{(1,1)}$ orbital solution. On the basis of independent radio-isotopic and orbital forcing results, we propose the refined age of 1.1850 ± 0.0016 Ma (2σ external uncertainty) for the Quaternary ACR $^{40}Ar/^{39}Ar$ sanidine standard.

1. Introduction

Obtaining concordant ages between the $^{40}Ar/^{39}Ar$ and $^{206}Pb/^{238}U$ radio-isotopic dating systems for a given geologic unit is an essential step towards improving the accuracy of the geologic time scale. Historically, there has been an offset of up to 1% between $^{40}Ar/^{39}Ar$ and U/Pb ages (e.g. Min et al., 2000; Schoene et al., 2006 and references therein), far greater than the necessary ±0.1% precision goal needed to construct an integrated, multi-chronometer geologic time scale (EARTHTIME initiative, www.earth-time.org).

An objective of EARTHTIME is to improve upon the accuracy and precision of neutron fluence monitors used in $^{40}Ar/^{39}Ar$ isotopic dating. Recent intercalibration efforts by a variety of techniques for the Fish Canyon sanidine (FCs) monitor have succeeded in reducing uncertainties to near the goal of ±0.1% in relative age (e.g. Kuiper et al., 2008; Renne et al., 2011; Rivera et al., 2011). Several studies have shown that by using an astronomically calibrated $^{40}Ar/^{39}Ar$ age for the monitor mineral, $^{40}Ar/^{39}Ar$ and U/Pb ages are within uncertainty over much of geologic time, and agreement between these chronometers can be achieved to a level of ±0.3% (Kuiper et al., 2008; Smith et al., 2010; Rivera et al., 2011; Meyers et al., 2012). For example, using sanidine extracted from the Miocene A1 tephra (Crete) astronomically dated at the precession scale, rather than intercalibration with primary or secondary $^{40}Ar/^{39}Ar$ standards or with U–Pb systematics, can minimize full systematic errors to the ca. ±0.1% level (Rivera et al., 2011).

In this contribution, we present an age for the Quaternary $^{40}Ar/^{39}Ar$ mineral dating standard Alder Creek Rhyolite (ACR) sanidine (Turrin et al., 1994) calibrated against A1 tephra sanidine (A1Ts), and reported with full systematic uncertainties to a precision of ±0.1%. ACR erupted

* Corresponding author at: Department of Geosciences, Boise State University, Boise, Idaho, USA.
E-mail address: tiffanyrivera@boisestate.edu (T.A. Rivera).

0009-2541/$ – see front matter © 2013 Elsevier B.V. All rights reserved.
http://dx.doi.org/10.1016/j.chemgeo.2013.02.021

during the Cobb Mountain normal polarity subchron (C1r.2n), within the Matuyama reverse polarity chron (Mankinen et al., 1978). Previously reported radio-isotopic ages for ACR and derived astronomical ages for the Cobb Mountain subchron are inconsistent. For example, reported $^{40}Ar/^{39}Ar$ sanidine ages range from 1.180 to 1.21 Ma (e.g. Coble et al., 2011; Renne et al., 2011), and ion probe $^{238}U/^{206}Pb$ zircon age peaks are 1.30 ± 0.04 Ma with a minor (<20%) sub-population at 1.50 ± 0.04 Ma (Schmitt et al., 2003a). Astronomical estimates for the subchron range from 1.173 to 1.215 Ma (e.g. Channell et al., 2002; Horng et al., 2002). The inconsistency in ages of ~0.2 Ma across these three techniques is undesirable and clouds interpretation of $^{40}Ar/^{39}Ar$ dates produced using ACR sanidine as the monitor mineral. In light of recent improvements in our knowledge of the age of the FCs monitor (Kuiper et al., 2008; Rivera et al., 2011), a re-evaluation of the Quaternary $^{40}Ar/^{39}Ar$ standard is timely.

This study uses a combined approach of $^{40}Ar/^{39}Ar$ sanidine and CA-TIMS $^{206}Pb/^{238}U$ zircon dating techniques to provide an eruption age for the ACR and associated Cobb Mountain subchron. Previous ion microprobe U–Pb studies of ACR zircon have highlighted the problems of significant age dispersion in individual zircon crystal ages of up to 200 ka older than the apparent eruption age (Schmitt et al., 2003a), one of many examples in the literature of small volume rhyolites where zircon records protracted magma residence or crystal recycling (e.g. Schmitt, 2011). Further, trace element concentrations in quartz-hosted melt inclusions demonstrated zircon undersaturation of the ACR magma, thus leading to the interpretation that most ACR zircon crystals are more likely recycled 'antecrysts' from re-melted plutonic precursors to the ACR magma, rather than recorders of prolonged shallow magma chamber evolution (Schmitt et al., 2003a).

In this work, we test the recycled antecryst hypothesis by employing a tandem in situ trace element (including titanium-in-zircon thermometry) and CA-TIMS dating approach guided by cathodoluminescence imaging to distinguish zircon crystal populations within the ACR magma. Specifically, we identify zircon crystals with low incompatible trace element concentrations, crystallization temperatures greater than the two-feldspar eruption temperature, and dates near the $^{40}Ar/^{39}Ar$ eruption age — those that could represent rapid nucleation and growth from an initially zircon undersaturated ACR magma hypothesized by Schmitt et al. (2003a). Additionally, we confirm older zircon crystals with lower temperatures and higher incompatible trace element concentrations as an antecrystic contribution to the crystal cargo, derived from the underlying Geysers Plutonic Complex. The discrimination of distinctive zircon crystal populations by age, temperature, and composition can clarify the relative importance of crystal residence in differentiating magmas (e.g., Reid et al., 1997) versus crystal recycling from precursor intrusive or extrusive rocks (e.g., Bindeman et al., 2001), in addition to providing critical supporting evidence for the eruption age of the ACR.

1.1. Geologic setting

Alder Creek Rhyolite (ACR) is the oldest unit of the Cobb Mountain felsic composite dome situated in the Geysers Geothermal-Clear Lake Volcanic Field within the Coast Ranges of Northern California. ACR has a transitional to normal geomagnetic polarity direction relative to the reverse directions of the younger Cobb Valley dacite and Cobb Mountain rhyodacite (Fig. 1; Mankinen et al., 1978). These three subaerial eruptive deposits overlay the eastern portion of the Geysers Plutonic Complex composed of granite and granodiorite that intruded into Mesozoic Franciscan Complex metagraywackes (Hulen and Nielson, 1993). The entire area has been attributed to a strike-slip basin that developed between fault segments associated with the San Andreas transform (Donnelly-Nolan et al., 1993) and is one of the world's largest producers of geothermal energy. Volcanism within the region has been attributed to asthenospheric upwelling associated with the termination of subduction as a result of the northward migration of the Mendocino Triple Junction (e.g. Stimac et al., 2001 and references within).

2. Materials and methods

We analyzed the widely distributed ACs-2 purified sanidine separate (Nomade et al., 2005) and zircon separated by standard magnetic and gravimetric techniques at Boise State University (BSU) from a bulk sample of ACR2 (Schmitt et al., 2003a, 2006). For simplicity, we use the notation of ACRs and ACRz to represent Alder Creek Rhyolite sanidine and zircon, respectively.

2.1. $^{40}Ar/^{39}Ar$ methodology

The ACRs experiments were conducted with Fish Canyon sanidine (FCs) and A1 tephra sanidine (A1Ts) as the neutron fluence monitors, using the astronomically calibrated ages of 28.172 ± 0.018 Ma and 6.943 ± 0.005 Ma (2σ), respectively (Rivera et al., 2011), which are tied to the ^{40}K partial decay constants of Min et al. (2000). Using sapropel cyclostratigraphic correlation, the A1 tephra of the Faneromeni section (Crete) was astronomically tuned to the $La2004_{(1,1)}$ precession scale with the La2010 eccentricity modulation (Hilgen et al., 1995; Laskar et al., 2004, 2011; Rivera et al., 2011). Kuiper et al. (2004) initially assigned an uncertainty of ±0.005 Ma to the A1 tephra, which was later argued to be equivalent to a statistically derived uncertainty of 2σ (Rivera et al., 2011). Calibration of the FCs monitor relative to the A1Ts resulted in an age and uncertainty of 28.172 ± 0.018 Ma (Rivera et al., 2011), which is adopted for this study.

Handpicked crystals of ACRs, FCs, and A1Ts were loaded into 21-pit aluminum irradiation disks using the bracketing geometries depicted in the Supplementary materials, Fig. A.1. The disks were wrapped in aluminum foil and heat-sealed within a quartz glass tube. Two irradiations were conducted at the cadmium-lined in-core (CLICIT) facility at the Oregon State University TRIGA reactor. Irradiation time for the ACRs-FCs ($ACRs_{FCs}$) intercalibration was 6 h (lab ID QL-OSU-20A), while the ACRs-A1Ts ($ACRs_{A1Ts}$) irradiation was 2 h (lab ID QL-OSU-22A).

Single crystal $^{40}Ar/^{39}Ar$ laser fusion analyses of ACRs were carried out on a Nu Instruments Noblesse multi-collector noble gas mass spectrometer housed at the Quaternary Dating Laboratory (QUADLAB), Roskilde University, following previously described methods (Storey et al., 2007; Brumm et al., 2010; Rivera et al., 2011; Storey et al., 2012). The Noblesse is equipped with one high-mass Faraday detector and three ETP ion-counting electron multipliers. ^{40}Ar and ^{39}Ar were measured on the Faraday detector, ^{38}Ar and ^{37}Ar on the axial ion counter, and ^{36}Ar on the low-mass ion counter (see Figure A.2 of Rivera et al., 2011). The detector configuration allowed for simultaneous measurement of ^{40}Ar, ^{38}Ar, and ^{36}Ar, followed by peak hopping to measure ^{39}Ar and ^{37}Ar. Dead time corrections for the axial and low mass ion counters were 37.1 ns and 23.7 ns, respectively (Brumm et al., 2010). The same detector configuration was used for analysis of monitors, unknowns, blanks, and atmospheric argon delivered from a calibrated pipette system, which was used to determine detector intercalibration and mass fractionation corrections (Fig. A.2; Brumm et al., 2010; Rivera et al., 2011; Storey et al., 2012). In the case of QL-OSU-22A, A1Ts was analyzed as multi-crystal fusion experiments of 3–4 grains to allow for more precise measurement of ^{39}Ar on the Faraday detector. Crystals were gently degassed prior to fusion using a defocused beam from a 50 W Synrad CO_2 laser, followed by total fusion at 4–12 W power with a focused beam. Weighted mean values for a 400 second full-system blank were 1.10×10^{-16} ± 1.2% mol ^{40}Ar (2σ; MSWD = 2.8; n = 159) and 1.36×10^{-18} ± 0.39% mol ^{36}Ar (2σ; MSWD = 2.0; n = 143) for QL-OSU-20A, and 1.17×10^{-16} ± 1.5% mol ^{40}Ar (2σ; MSWD = 1.9; n = 109) and 1.12×10^{-18} ± 0.54% mol ^{36}Ar (2σ; MSWD = 1.3; n = 100) for QL-OSU-22A. Interfering isotope corrections are the same as those used in Rivera et al. (2011). Data collection and

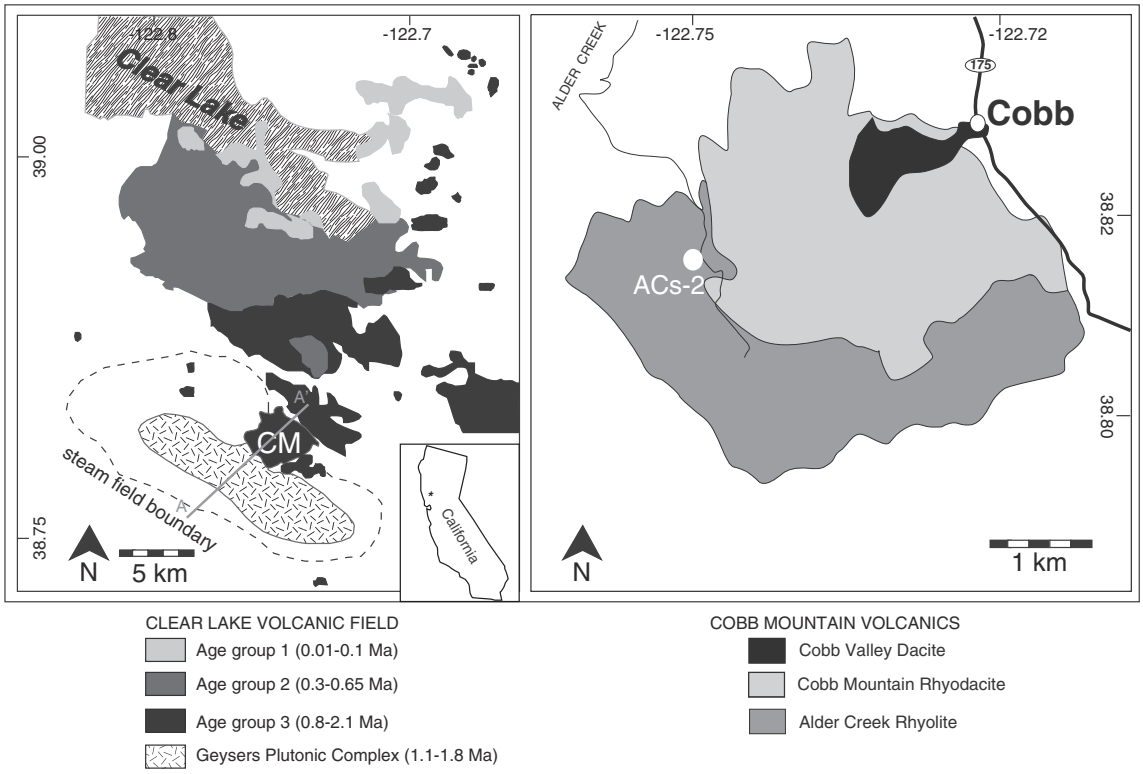

Fig. 1. Left: Location map of Cobb Mountain (CM) within the context of the Geysers-Clear Lake Volcanic Field with ages of volcanic products shown. Approximate location of the geothermal steam field boundary is indicated. Right: Sketch map of the volcanic units at Cobb Mountain shown with the sample location of ACs-2, which is the same sample used in this study (ACRs). Maps modified from Schmitt et al. (2003a) and Nomade et al. (2005).

reduction were carried out using the program MASS SPEC (A. Deino, Berkeley Geochronology Center).

2.2. U–Pb methodology

Zircon crystals mounted in epoxy were ground to expose a medial section of each grain, followed by cathodoluminescence (CL) imaging at BSU (Fig. B.1). A second grain mount was prepared and imaged at the University of California Los Angeles (UCLA, Fig. B.1). Guided by CL images, trace element concentrations and preliminary $^{238}U/^{206}Pb$ dates were obtained by LA-ICPMS, using 40 μm laser spots on the BSU zircon mount. Laser spots of 30 μm were used to re-occupy the same location within the UCLA zircon crystals where an earlier ion microprobe analysis was conducted (A. Schmitt; unpublished data). A total of 47 laser spots were placed on 43 grains. Further details on methodology, instrumentation, laser and mass spectrometer parameters, calibration standards, and sample data are given in the Supplementary materials.

After trace element characterization and LA-ICPMS $^{238}U/^{206}Pb$ date determinations, selected crystals were extracted from the mounts for chemical abrasion thermal ionization mass spectrometry (CA-TIMS) analysis (Mattinson, 2005), spiked with EARTHTIME isotope dilution tracer solutions (ET535 or ET2535; Condon et al., 2007). Procedures for annealing, dissolution, chemical separation, and mass spectrometry follow those described by Davydov et al. (2010). A total of 24 CA-TIMS analyses were performed on an IsotopX Isoprobe-T mass spectrometer at BSU. Calculation of U–Pb dates and uncertainties follow the equations presented in Schmitz and Schoene (2007) and utilize the U decay constants of Jaffey et al. (1971). All $^{238}U/^{206}Pb$ dates reported and discussed here were corrected for Th/U disequilibrium using a $Th/U_{[magma]}$ value of 2.3 ± 0.6 (2σ) based on the average of ACR quartz-hosted melt inclusions and whole rock analyses (Schmitt et al., 2003a). The ACR magma was assumed to be in secular equilibrium with respect to $^{230}Th/^{238}U$ and thus the reported ages may overestimate the true crystallization ages by 4 ka per 5% ^{230}Th excess, recognizing that magmatic $^{230}Th/^{238}U$ activity ratios greater than unity (up to 1.1) are often measured in Pleistocene to Holocene rhyolites (Jicha et al., 2007; Reagan et al., 2003; Lowenstern et al., 2006). Common Pb (up to 0.4 ± 0.2 pg) was attributed to procedural blank with a composition of $^{206}Pb/^{204}Pb = 18.04 \pm 1.28\%$, $^{207}Pb/^{204}Pb = 15.54 \pm 1.10\%$, and $^{208}Pb/^{204}Pb = 37.67 \pm 1.28\%$ (2σ). Any remaining common Pb was assigned to initial Pb, with a composition determined on a co-existing feldspar mineral separate (Table 2; Table B.3). Further details on methods, instrumentation, mass fractionation and isobaric interference corrections, standards, and laboratory and initial Pb compositions are given in the Supplementary materials.

3. Results

3.1. $^{40}Ar/^{39}Ar$ sanidine age determinations

Eighty-eight single crystal fusion analyses of ACRs were conducted relative to the two monitor minerals. On average, the A1Ts ^{36}Ar signal was six times greater than the blank analyses, while the ACRs signal was approximately twice the size of the blank analyses. In general, grains of ACRs were highly radiogenic with $^{40}Ar^*$ typically greater than 90%, and analyses with less than 70% $^{40}Ar^*$ were considered outliers. Additionally, following Kuiper et al. (2008), data were rejected from calculations if Ca/K was greater than 1 or if ^{39}Ar was less than 5×10^{-16} mol. Finally, analyses with a normalized median absolute deviation (nMAD) greater than 1.5 were considered outliers (Powell et al., 2002). These outlier criteria were applied to both ACRs and monitor analyses. *J*-values were calculated by fitting a plane through the neighboring positions of FCs or A1Ts using the algorithms of the MASS SPEC software (A. Deino, Berkeley Geochronology Center).

The intercalibration results presented in Table 1 are inverse variance weighted mean ages with associated errors at the 2σ level. For

consistency across dating techniques, all uncertainties are reported at the 2σ level unless otherwise stated. Age-probability distribution plots for each experiment are shown in Fig. 2. $ACRs_{FCs}$ experiments (QL-OSU-20A) result in a model age of 1.1850 ± 0.0010 Ma (including errors on *J*). The $ACRs_{A1Ts}$ intercalibration experiment (QL-OSU-22A) yields an inverse variance weighted mean age of 1.1854 ± 0.0040 Ma (including errors on *J*). Using the intercalibration factor $\left(R^{FCs}_{A1Ts} = \frac{(e^{\lambda_{total}{}^{FCs}} - 1)}{(e^{\lambda_{total}{}^{A1Ts}} - 1)}\right)$ determined by Rivera et al. (2011), the $ACRs_{FCs}$ ages are recalculated relative to A1Ts. Then a weighted mean age of all single crystal analyses from the two experiments was calculated to determine our preferred age for ACRs of 1.1850 ± 0.0016 Ma (external errors), which translates to an R^{ACRs}_{A1Ts} value of 0.17041 ± 0.00019. External error propagation methods follow the algorithms of Kuiper et al. (2008). Alternatively, recalculating the $ACRs_{A1Ts}$ experiments to the FCs monitor results in a value of 0.041754 ± 0.000030 for R^{ACRs}_{FCs}. This value is consistent with that determined on the QUADLAB aliquot of the 2008 EARTHTIME intercalibration experiment (0.04182 ± 0.00014; Heizler and EARTHTIME Ar working group, 2008; Storey et al., 2012) and that determined by experiments conducted using a different methodology at Stanford University (0.04182 ± 0.00018; Coble et al., 2011). Blank-corrected raw data are presented in Tables A.1 and A.2 and outlier detection plots for monitors are shown in Fig. A.3.

Our intercalibration results are further supported when the data are cast upon an $^{39}Ar/^{40}Ar$ versus $^{36}Ar/^{40}Ar$ correlation plot. The inverse isochron ages are statistically consistent with the weighted mean ages (Fig. 3). Further, regression of the data for each experiment yields $^{40}Ar/^{36}Ar$ values of 300.4 ± 7.7 and 303.9 ± 4.6, which are in general agreement with the published atmospheric ratio (Lee et al., 2006).

3.2. Zircon trace element analyses, thermometry, and LA-ICPMS $^{238}U/^{206}Pb$ dates

Zircon trace element signatures have been used to determine the composition of the parental melt and associated crystallizing phases, such as garnet, monazite, and feldspars, as well as metamorphic events, or provenance in detrital settings (e.g. Hinton and Upton, 1991; Hoskin and Ireland, 2000; Rubatto, 2002). Concurrently, titanium abundance within the zircon crystal lattice can serve as a proxy for the temperature of the magma at the time of crystallization (Watson and Harrison, 2005; Watson et al., 2006; Ferry and Watson, 2007). Thus, in situ trace element analyses by LA-ICPMS coupled with the isotopic dating approach allows for discerning the crystallization history and petrologic significance of a chemically and thermally evolving rhyolite system, while simultaneously placing these events into a temporal context.

ACRz were initially divided into two groups based upon their physical and CL characteristics (Fig. 6; Fig. B.1). Group A zircon crystals represent a minor component of the population, tend to be highly elongate in shape, generally lack a sharply defined zoning pattern, and often contain a bright interior surrounded by a thin darker overgrowth. Conversely, Group B zircon crystals are more abundant, more equant in form, exhibit an obvious oscillatory zoning pattern, and are relatively darker in CL from core to rim compared to Group A zircon.

The morphological groupings are apparent in the chemical compositions. Fig. 4 shows a selection of trace element concentrations and ratios, as well as titanium-in-zircon (TiZR) temperatures for the analyzed laser spots. TiZR temperatures were obtained using the equations of Ferry and Watson (2007) for a rutile-absent melt. We assume an activity of 1 for α_{SiO_2} and 0.55 for α_{TiO_2}. The TiO_2 activity is an estimation based on other TiO_2 activities for large-volume silicic volcanic units in the western United States (e.g. Reid et al., 2011; Wark et al., 2007; Hayden and Watson, 2007; Campbell et al., 2009). Analytical uncertainties on TiZR temperatures are ±10 °C, determined by repeated analysis of the Orapa (Botswana) kimberlite standard (Fig. B.2). Similarly, a variation of ±10% in the value chosen for α_{TiO_2} results in an uncertainty on TiZR temperatures of ±10 °C. Zircon trace element data and thermometry results are presented in Tables B.1 and B.2.

The bivariate plots in Fig. 4 demonstrate the compositional differences between Group A and Group B zircon crystals. While a number of trace element parameters, including Hf concentrations, total REEs, Eu anomalies, or TiZR temperatures may be used to monitor changes in the magmatic environment from which zircon is crystallizing, we introduce Th/Y as an additional monitor of magmatic differentiation. Th/Y will vary in silicic magmas due to the large relative difference in incompatibility of these two elements between crystals and silicic melts. Assuming both elements remain incompatible, a more differentiated, low-T, high silica rhyolite will evolve to greater values of Th/Y. By contrast, magmas saturated in a Th-rich phase, such as titanite, allanite, or chevkinite, may evolve to lower Th/Y. In either scenario, this trace element ratio should exhibit substantial variations during progressive differentiation of an individual melt batch, or between distinct magmas. The use of a trace element ratio is advantageous from an analytical perspective, as ratios are generally more precisely and accurately measured via in situ laser and microbeam techniques. Fig. 4 demonstrates how Th/Y covaries in a predictable manner with other trace elements in zircon.

Group A zircon generally trend towards lower Th/Y (<0.3), higher crystallization temperatures (720–840 °C; Fig. 4A), smaller negative Eu anomalies (higher values for Eu/Eu*; Fig. 4B; Trail et al., 2012), and lower concentrations of incompatible elements, including Nb and Hf (Fig. 4D and E). Conversely, Group B zircon trend towards higher Th/Y (>0.3), cooler crystallization temperatures (670–800 °C), larger negative Eu anomalies (lower values for Eu/Eu*), and higher incompatible trace element concentrations. Within each group, Th/Y is positively correlated with Hf and Nb concentrations, and more weakly negatively correlated with TiZR temperature and Eu anomaly. These correlations are consistent with the hypothesis of continued incompatibility and progressive enrichment of the actinides, lanthanides, and high-field strength elements during cooling and crystallization of the parental magmas of both Group A and B zircon. Although this study did not focus on detailed intracrystalline trace element profiles, relative CL

Table 1
Summary of Alder Creek Rhyolite sanidine $^{40}Ar/^{39}Ar$ dating results.

Weighted mean results

Run series	Monitor	T (Ma)	±2σ internal, %	±2σ internal with *J*, %	±2σ external, %	MSWD, prob	n	R ±2σ error
QL-OSU-20A	FCs	1.1850	0.0008, 0.08%	0.0010, 0.08%	0.0014, 0.12%	1.33, 0.14	29/34	0.041754, 0.000042
QL-OSU-22A	A1Ts	1.1854	0.0008, 0.06%	0.0040, 0.34%	0.0044, 0.36%	1.01, 0.49	46/54	0.170462, 0.000616
Combined	A1Ts	1.1850			0.0016, 0.14%			0.170413, 0.000194

Inverse isochron results

Run series	Monitor	T (Ma)	±2σ internal with *J*, %	$^{40}Ar/^{36}Ar$ ± 2σ	MSWD	n
QL-OSU-20A	FCs	1.1846	0.0019, 0.16%	300.4 ± 7.7	1.5	29/34
QL-OSU-22A	A1Ts	1.1850	0.0041, 0.35%	303.9 ± 4.6	1.4	46/54

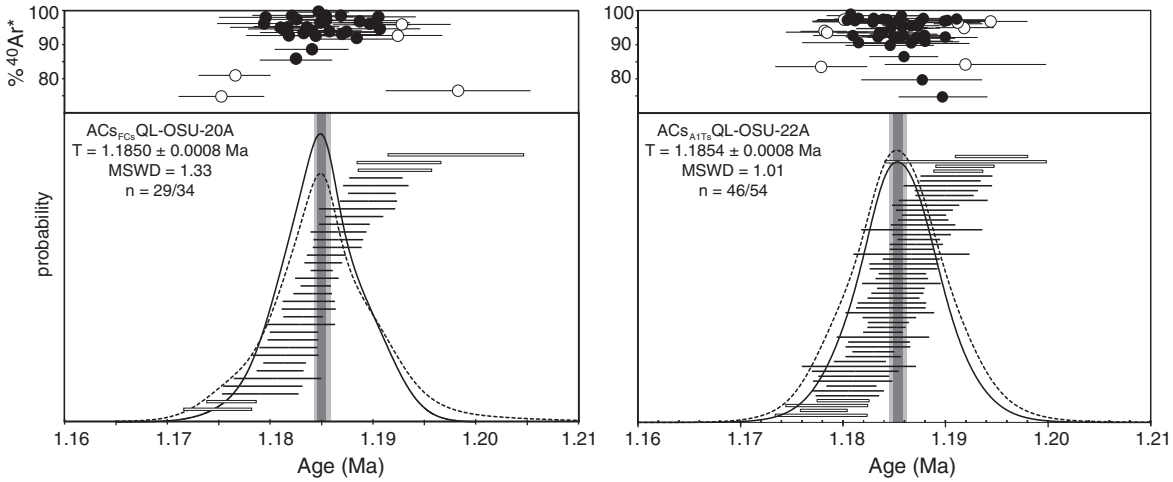

Fig. 2. $^{40}Ar/^{39}Ar$ single crystal Alder Creek Rhyolite sanidine age probability distributions and percent $^{40}Ar^*$ of QL-OSU-20A and QL-OSU-22A. Open symbols indicate outliers. The dashed line represents the distribution if outliers were included. Individual analyses are shown with one-sigma errors. Weighted mean ages with one- and two-sigma analytical uncertainties are indicated by dark and light vertical bars, respectively.

intensities within crystals also support a general increase in these elements from core to rim, albeit complicated by oscillatory zoning in the Group B zircon.

Fig. 4C illustrates the covariation in Th/U versus Th/Y between and within the two groups. Trace element ratios can provide a clearer distinction between discrete zircon populations as they are analytically more robust. Random signal fluctuations during ablation common to both ratioed elements are canceled out, and ratios accentuate magmatic source signatures over differentiation enrichments. Although some degree of auto-correlation is expected when comparing Th/U and Th/Y, the separation and contrasting slopes of the data trends clearly distinguish Group A from Group B. The small number of intermediate compositions between the two arrays may represent mixed analyses from laser spots that overlap Group B cores and Group A overgrowths.

ACRz exhibit chondrite-normalized REE patterns similar to those of other magmatic zircon, with pronounced negative Eu and positive Ce anomalies coupled to an enrichment of light REE (Fig. 5). Compared to Group A zircon, Group B zircon have more pronounced Ce and Eu anomalies, more uniform REE contents and patterns, and exhibit steeper middle to heavy REE slopes. A subset of Group B ($n = 4$) displays a relatively flat light REE pattern at ca. 100 times enrichment over the CI chondrite. Although the time-resolved ablation signals were screened for glass or mineral inclusions (e.g. excess P or Ti counts), these light REE enrichments may still be due to micro-inclusions.

LA-ICPMS geochronology is challenging in such young zircon crystals with minor amounts of ingrown radiogenic Pb. Individual spots yielded absolute uncertainties of 50 to 200 ka (2σ) depending upon U concentration. Experiments with differing common Pb correction schemes (204-, 207-, and 208-Pb corrections) were limited by the Hg interference

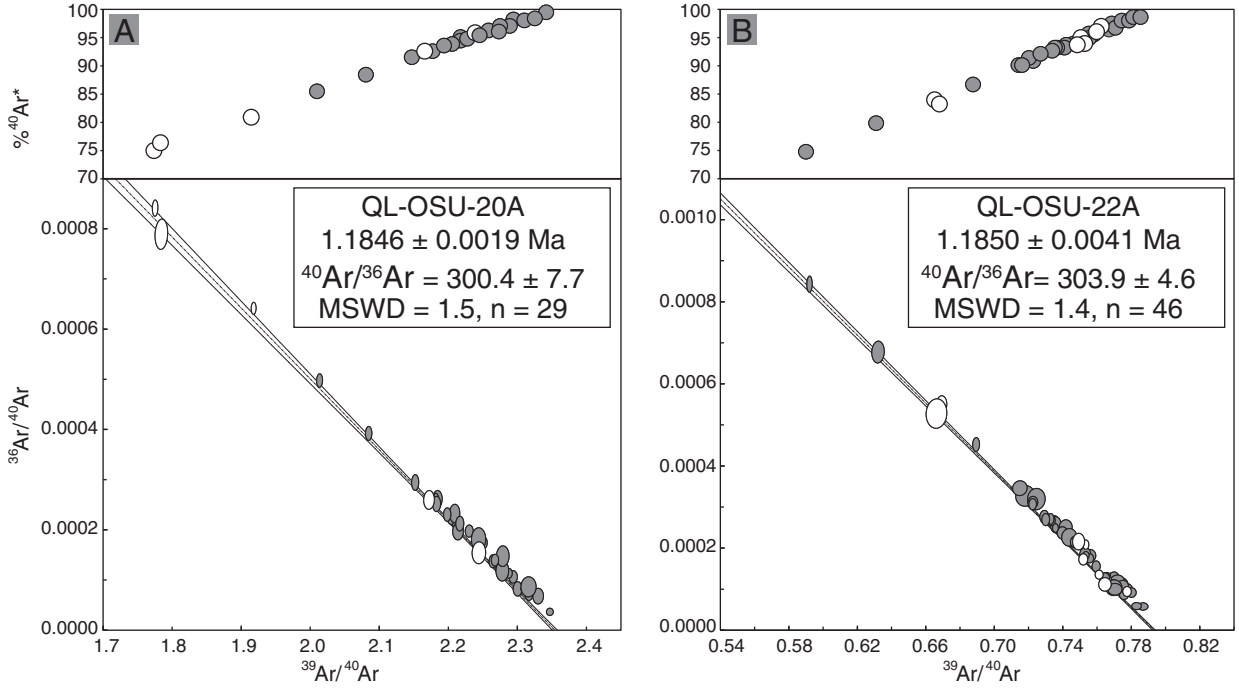

Fig. 3. $^{40}Ar/^{39}Ar$ inverse isochron diagrams for Alder Creek Rhyolite sanidine. A) QL-OSU-20A; B) QL-OSU-22A. Symbols are shown with 2σ correlated error ellipses using the algorithms of Schmitz and Schoene (2007). Open symbols represent rejected analyses. For reference, the upper panel shows percent $^{40}Ar^*$ for each analysis plotted on the isochron. Ages are shown with 2σ analytical (including J) uncertainties.

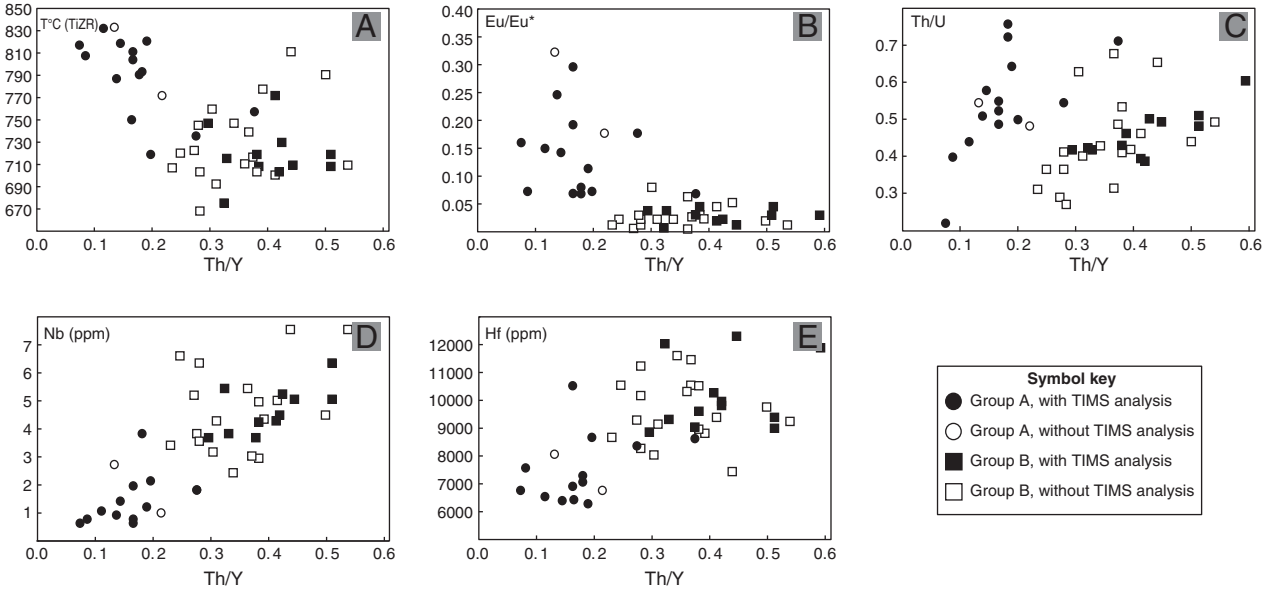

Fig. 4. Bivariate plots of selected trace element and TiZR temperatures for Alder Creek Rhyolite zircon crystals.

on mass 204 and the very low count rates for ^{207}Pb and ^{208}Pb; we report and illustrate the ^{206}Pb/^{238}U dates with no common Pb correction in the Supplementary materials, Tables B.1 and B.2 and Fig. B.3. Despite the low radiogenic Pb contents, 37 concordant spot dates yield a probability density function with an asymmetric distribution described by a median ^{206}Pb/^{238}U date of 1.17 +0.09/−0.03 Ma. As will be illustrated in the next section, these in situ results are consistent within their large errors with the conclusions drawn from high-precision CA-TIMS analyses.

3.3. CA-TIMS U–Pb age determinations

Trace element concentrations were used to select 22 zircon crystals from Group A and Group B for CA-TIMS analysis (Fig. 6). The majority of Group A crystals are from the larger population of grains in the BSU mount; only one (ACR2-g8; z22) of ten crystals in the UCLA mount had the low trace element compositions typical of Group A. Two large elongate Group A crystals were broken to allow for multiple dates from a single zircon and are labeled as such in Fig. 6. The ACRz CA-TIMS ^{206}Pb/^{238}U dates, corrected for Th/U disequilibrium, range from 1.377 ± 0.004 Ma to 1.166 ± 0.028 Ma (analytical error) indicating apparent zircon crystallization over at least 200 ka. However, the geochemically distinct Group A and B zircon are distinguished by younger and older ages, respectively (Table 2). Group B dates are between 1.377 and 1.239 Ma, while Group A dates are between 1.231 and 1.166 Ma. The nine youngest crystals define a weighted mean age of 1.1978 ± 0.0043/0.0046 Ma (analytical/systematic error; MSWD = 0.84, p = 0.57; Fig. 6). This cluster includes the five crystals yielding the highest TiZR temperatures, as well as those analyses that are analytically indistinguishable from that cluster. An additional four analyses of Group A zircon with resolvably older dates may be excluded objectively based upon a combination of lower TiZR temperatures, higher incompatible trace element concentrations and ratios, and complexities in their CL imaging patterns (see Discussion below). This includes one fragment from crystal z11, suggesting that the older ages may be the result of heterogeneous nucleation of Group A zircon on Group B cores.

4. Discussion

Coupled ACR ^{40}Ar/^{39}Ar sanidine eruption ages and high-precision ^{206}Pb/^{238}U zircon dates, whose compositions also record pre-eruptive thermal and chemical conditions, are powerful tools for understanding the timescales and mechanisms of felsic magma differentiation. In particular, the zircon CA-TIMS dates used in combination with the TiZR geothermometer (Ferry and Watson, 2007) offer the possibility of precisely constraining the thermal evolution of the ACR magma prior to eruption. In this section, we discuss the implications of two chemically distinct ACRz populations, the eruption age as determined through ^{40}Ar/^{39}Ar dating, and the broader implications on the age of the Cobb Mountain subchron.

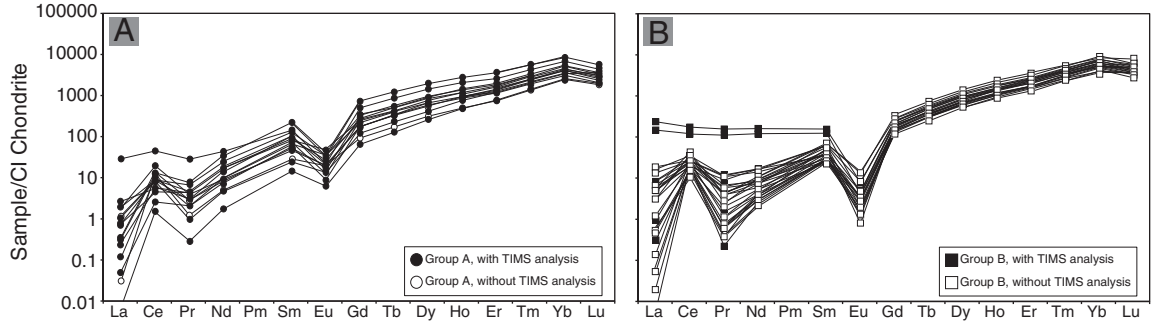

Fig. 5. Chondrite-normalized REE diagram for Alder Creek Rhyolite zircons.

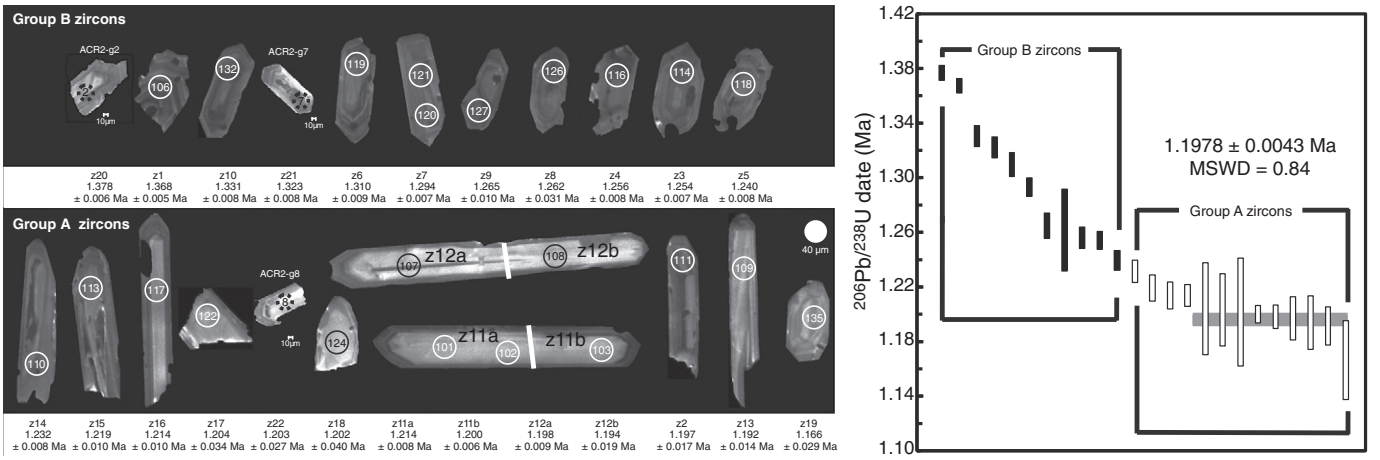

Fig. 6. Left: Selected CL images of Alder Creek Rhyolite zircon crystals with their respective CA-TIMS dates. Right: Distribution of CA-TIMS ages ranked by decreasing age. Group B zircon are represented by closed symbols; Group A zircon are represented by open symbols.

4.1. ACR zircon crystallization history

Several chemically and petrographically distinct intrusive phases comprise the Geysers Plutonic Complex, which is entirely subsurface, and only encountered in numerous geothermal drill wells (e.g. Dalrymple et al., 1999; Schmitt et al., 2003b; Fig. 8). One of these wells, GDC21, offered the best material to constrain the temporal and compositional relationships among the intrusive units (refer to Figure 2 of Schmitt et al., 2003b). Schmitt et al. (2003b) report that the oldest unit, a microgranite porphyry, is found in the shallowest depths, and yields $^{238}U/^{206}Pb$ zircon ion microprobe (IMP) dates ranging from 1.63 to 1.91 Ma. An intermediate aged (1.46 ± 0.03 Ma) orthopyroxene-biotite granite is found at slightly deeper depths; however, the main intrusive phase is characterized by a second, compositionally distinct orthopyroxene-biotite granite (1.27 ± 0.01 Ma) and a granodiorite (1.25 ± 0.01 Ma). Within the depth range of the granite and granodiorite, but on the eastern lobe of the pluton, the youngest phase of plutonism resides below the Cobb Mountain volcanics and is characterized by a third, distinct orthopyroxene-biotite granite with an age of 1.16 ± 0.01 Ma (sample CA5636 74F 21, depths of 1900–2800 mbsl). Schmitt et al. (2003b) recognized that this particular granite was fresh, lacking chloritization, and contains a higher abundance of alkali feldspar relative to the other granites sampled. Finally, a felsic dike with an IMP age of 1.11 ± 0.03 Ma intrudes metagraywacke deposits, which underlie the Cobb Mountain volcanics. Within this framework, we draw correlations between the two groups of ACRz identified in this study and the phases of magmatism as recognized by Schmitt et al. (2003b).

4.1.1. Pre-ACR Group B zircon

The prismatic, oscillatory zoned, Group B zircon represent a period of abundant zircon crystallization from a fractionated, low-temperature, relatively homogeneous granitic magma. Group B zircon dated by CA-TIMS have a narrow range of TiZR temperatures (700–750 °C ± 10 °C), which are relatively constant over the ca. 140 ka of crystallization. On average, the TiZR temperatures calculated for this suite (670–800 °C ± 10 °C; average of 730 °C) are somewhat lower than the two-feldspar thermometry (750–780 °C) and zircon saturation temperatures (775–790 °C) for the ACR (Schmitt et al., 2003a). This temperature discrepancy would imply disequilibrium between the Group B zircon and the ACR magma. Further, this disequilibrium underscores the discrepancy in age between the ca. 1.38 to 1.24 Ma Group B zircon and the 1.185 Ma sanidine $^{40}Ar/^{39}Ar$ age of ACR eruption.

CA-TIMS dates from Group B are coincident with the IMP dates determined for the main phase of orthopyroxene-biotite granite intrusion into the shallow crust beneath the Geysers–Cobb Mountain Volcanic Field (Schmitt et al., 2003b). We interpret the Group B grains as crystallization products of this relatively homogeneous, low temperature (~730 °C) granitic magma body, residing at a shallow crustal depth, with crystallization occurring from 1.38 to 1.24 Ma. Thus, we define Group B zircon as antecedent to the production of the ACR magma, and scavenged during later partial melting of intrusives within the Geysers Plutonic Complex. These data and interpretations provide new evidence consistent with the conclusions of Schmitt et al. (2003a) that the Cobb Mountain eruptives represent partial remelting of earlier intrusives of the Geysers Plutonic Complex.

4.1.2. ACR-related Group A zircon

The elongate, weakly zoned, Group A zircon record a different chemical and thermal magmatic regime compared to Group B. For example, Group A zircon have lower incompatible element concentrations and less pronounced Ce and Eu anomalies (Figs. 4 and 5), characteristics of a less fractionated source magma. TiZR temperatures for Group A zircon are also consistently higher (720–840 °C; average of 790 °C) than those for Group B (Fig. 4; Tables B.1 and B.2). The TiZR temperatures (>800 °C) of bright central domains in Group A slightly exceed the whole rock calculated zircon saturation temperatures for ACR (780 °C) while the lower end of the Group A temperature range is in general agreement with the two-feldspar thermometry estimates of eruptive crystallization temperatures from 750 °C to 780 °C (Schmitt et al., 2003a). These thermochemical features are consistent with the Group A zircon recording the injection and differentiation of initially hotter, more mafic ACR magma into the Geysers–Cobb Mountain system. This is demonstrated by the correlation of the Eu anomaly and TiZR characteristics with overall younger CA-TIMS dates (Fig. 7); the weighted mean CA-TIMS $^{206}Pb/^{238}U$ date of 1.1978 ± 0.0046 Ma is the mean age of this ACR magma differentiation.

We interpret the apparently oldest Group A zircon crystals as physical mixtures with Group B cores. Complex zoning in the oldest Group A crystals (i.e. z14, z15, z16 at 1.21–1.23 Ma; Fig. 6) and an apparent mixing trend of increasing crystallization temperature (750–840 °C) with decreasing age support this interpretation (Fig. 7). By contrast, an alternative model that the dispersion in Group A dates is due to progressive crystallization during differentiation can be rejected on the basis of the apparent temperature increase to younger ages. Mixing of two co-existing melts over timescales of tens of thousands of years is also unlikely as zircon crystals from the cooler, more silicic magma would be

Table 2
Summary of $^{206}Pb/^{238}U$ Alder Creek Rhyolite zircon CA-TIMS dating experiments.

	Compositional parameters						Radiogenic isotope ratios								Isotopic ages					
Sample[a]	Th/U[b]	$^{206}Pb^*$ $\times10^{-13}$ mol[c]	mol% $^{206}Pb^*$[c]	Pb^*/Pb_c[c]	Pb_c (pg)[c]	$^{206}Pb/^{204}Pb$[d]	$^{208}Pb/^{206}Pb$[e]	$^{207}Pb/^{206}Pb$[e]	% err[f]	$^{207}Pb/^{235}U$[e]	% err[f]	$^{206}Pb/^{238}U$[e]	% err[f]	Corr. coef.	$^{207}Pb/^{206}Pb$[g]	±[f]	$^{207}Pb/^{235}U$[g]	±[f]	$^{206}Pb/^{238}U$[g]	±[f]
Group B																				
z20	0.328	0.0594	91.89%	3.29	0.43	223	0.113	0.0487	2.3	0.001434	2.5	0.0002137	0.402	0.648	131	52	1.45	0.04	1.3775	0.0055
z1	0.354	0.0659	93.78%	4.40	0.36	290	0.122	0.0495	2.2	0.001447	2.4	0.0002122	0.398	0.630	170	51	1.47	0.04	1.3680	0.0054
z10	0.360	0.0295	87.99%	2.15	0.33	150	0.124	0.0511	5.5	0.001454	5.8	0.0002065	0.587	0.499	244	124	1.48	0.09	1.3310	0.0078
z21	0.308	0.0335	84.70%	1.60	0.50	119	0.107	0.0479	7.0	0.001355	7.3	0.0002052	0.579	0.509	94	161	1.37	0.10	1.3227	0.0077
z6	0.413	0.0290	83.47%	1.51	0.47	110	0.142	0.0532	6.5	0.001490	6.7	0.0002032	0.685	0.478	336	143	1.51	0.10	1.3099	0.0090
z7	0.396	0.0380	90.32%	2.77	0.34	186	0.137	0.0516	3.5	0.001429	3.8	0.0002007	0.529	0.559	270	79	1.45	0.05	1.2936	0.0068
z9	0.418	0.0223	84.65%	1.65	0.34	118	0.144	0.0549	8.9	0.001486	9.1	0.0001963	0.754	0.409	408	194	1.51	0.14	1.2651	0.0095
z8	0.531	0.0046	57.98%	0.43	0.28	43	0.183	0.0651	108	0.001758	109	0.0001958	2.458	0.095	778	2228	1.78	1.93	1.2619	0.0310
z4	0.405	0.0297	87.55%	2.09	0.35	145	0.140	0.0522	5.2	0.001403	5.5	0.0001949	0.634	0.547	294	115	1.42	0.08	1.2563	0.0080
z3	0.372	0.0361	89.76%	2.58	0.34	176	0.129	0.0510	3.6	0.001368	3.9	0.0001946	0.534	0.582	241	81	1.39	0.05	1.2542	0.0067
z5	0.366	0.0216	87.97%	2.15	0.25	150	0.127	0.0518	6.0	0.001373	6.2	0.0001923	0.604	0.521	275	133	1.39	0.09	1.2395	0.0075
Group A																				
z14	0.478	0.0357	86.51%	1.95	0.46	135	0.165	0.0474	5.1	0.001249	5.3	0.0001911	0.664	0.546	70	117	1.27	0.07	1.2318	0.0082
z15	0.640	0.0394	86.12%	1.97	0.52	132	0.220	0.0457	6.3	0.001192	6.5	0.0001892	0.776	0.467	−19	149	1.21	0.08	1.2194	0.0095
z16	0.358	0.0226	80.23%	1.19	0.46	92	0.124	0.0494	11.6	0.001282	11.9	0.0001884	0.809	0.387	166	263	1.30	0.15	1.2141	0.0098
z11a	0.328	0.0317	68.87%	0.65	1.17	60	0.114	0.0504	14.2	0.001308	14.3	0.0001884	0.663	0.321	212	318	1.33	0.19	1.2141	0.0080
z17	**0.427**	**0.0060**	**51.57%**	**0.32**	**0.47**	**38**	**0.148**	**0.0638**	**207**	**0.001645**	**207**	**0.0001868**	**2.780**	**0.067**	**736**	**4262**	**1.67**	**3.45**	**1.2043**	**0.0335**
z22	**0.250**	**0.0075**	**55.82%**	**0.36**	**0.49**	**41**	**0.087**	**0.0537**	**118**	**0.001383**	**118**	**0.0001867**	**2.192**	**0.114**	**359**	**2582**	**1.40**	**1.66**	**1.2034**	**0.0264**
z18	**0.107**	**0.0050**	**48.25%**	**0.25**	**0.44**	**35**	**0.038**	**0.0463**	**456**	**0.001190**	**456**	**0.0001864**	**3.265**	**0.051**	**14**	**10532**	**1.21**	**5.50**	**1.2017**	**0.0392**
z11b	**0.319**	**0.0376**	**88.99%**	**2.34**	**0.39**	**164**	**0.111**	**0.0483**	**4.5**	**0.001241**	**4.8**	**0.0001862**	**0.533**	**0.562**	**115**	**103**	**1.26**	**0.06**	**1.2002**	**0.0064**
z12a	**0.306**	**0.0255**	**79.73%**	**1.14**	**0.53**	**90**	**0.107**	**0.0482**	**13.4**	**0.001236**	**13.6**	**0.0001859**	**0.726**	**0.332**	**110**	**305**	**1.25**	**0.17**	**1.1983**	**0.0087**
z2	**0.551**	**0.0110**	**72.69%**	**0.83**	**0.34**	**66**	**0.190**	**0.0568**	**31.7**	**0.001453**	**32.0**	**0.0001857**	**1.387**	**0.210**	**482**	**682**	**1.47**	**0.47**	**1.1971**	**0.0166**
z12b	**0.409**	**0.0104**	**65.43%**	**0.56**	**0.45**	**53**	**0.142**	**0.0507**	**67.2**	**0.001295**	**67.5**	**0.0001852**	**1.617**	**0.143**	**227**	**1506**	**1.31**	**0.89**	**1.1940**	**0.0193**
z13	**0.316**	**0.0148**	**64.96%**	**0.54**	**0.66**	**53**	**0.110**	**0.0483**	**47.8**	**0.001232**	**48.0**	**0.0001849**	**1.171**	**0.167**	**116**	**1090**	**1.25**	**0.60**	**1.1916**	**0.0140**
z19	**0.224**	**0.0068**	**52.56%**	**0.31**	**0.51**	**39**	**0.079**	**0.0507**	**215**	**0.001265**	**215**	**0.0001810**	**2.447**	**0.075**	**227**	**4790**	**1.28**	**2.76**	**1.1664**	**0.0285**

[a] z1, z2 etc. are labels for single zircon crystals or fragments annealed and chemically abraded after Mattinson (2005). z1–z10 were spiked with the ET535 tracer, and z11–z22 with the ET2535 tracer. Samples in bold along with their corresponding values were used in the weighted mean age calculation.

[b] Model Th/U ratio iteratively calculated from radiogenic $^{208}Pb/^{206}Pb$ ratio and apparent $^{206}Pb/^{238}U$ age.

[c] Pb^* and Pb_c represent radiogenic and common Pb, respectively; mol% $^{206}Pb^*$ with respect to radiogenic, blank and initial common Pb.

[d] Measured ratio corrected for spike and fractionation only. Fractionation of U and Pb determined using the double spike composition of the ET2535 tracer, or (for Pb) estimated at 0.15 ± 0.03%/a.m.u. for ET535 based on over 600 analyses of ET2535-spiked zircons.

[e] Corrected for fractionation, spike, and common Pb; common Pb up to 0.4 pg was assumed to be procedural blank: $^{206}Pb/^{204}Pb = 18.04 \pm 0.64\%$; $^{207}Pb/^{204}Pb = 15.54 \pm 0.55\%$; $^{208}Pb/^{204}Pb = 37.67 \pm 0.64\%$ (all uncertainties 1-sigma). Excess over blank was assigned to initial common Pb, using the measured composition of co-existing feldspar: $^{206}Pb/^{204}Pb = 19.11 \pm 0.04\%$; $^{207}Pb/^{204}Pb = 15.62 \pm 0.07\%$; $^{208}Pb/^{204}Pb = 38.78 \pm 0.09\%$ (all uncertainties 1-sigma).

[f] Errors are 2-sigma, propagated using the algorithms of Schmitz and Schoene (2007).

[g] Calculations are based on the decay constants of Jaffey et al. (1971). $^{206}Pb/^{238}U$ and $^{207}Pb/^{206}Pb$ ages corrected for initial disequilibrium in $^{230}Th/^{238}U$ using Th/U [magma] = 2.3 (Schmitt et al., 2003a).

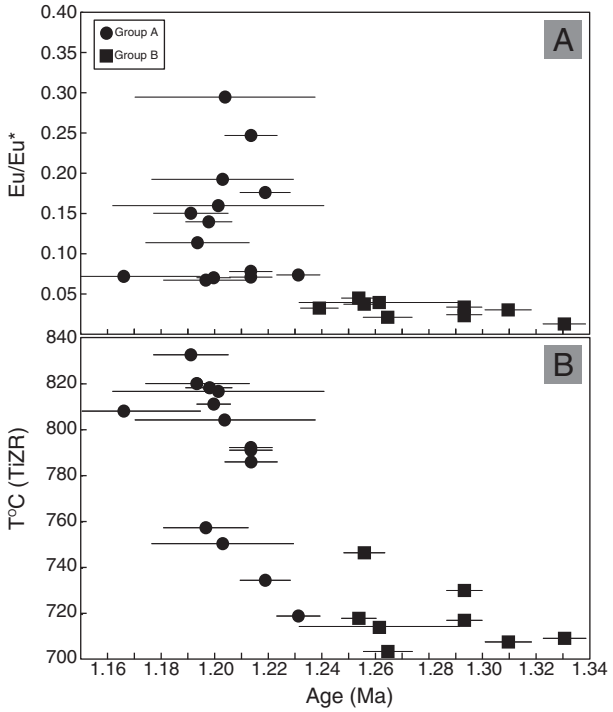

Fig. 7. Eu anomaly and TiZR temperatures versus CA-TIMS date for Alder Creek Rhyolite Group A and B zircon. Error bars are 2σ analytical uncertainties.

more likely to dissolve upon mixing with a hotter, Zr undersaturated mafic magma than undergo additional growth. The preferred model of antecrystic cores with younger overgrowths is further evidenced by the chemistry, thermometry, and dates within single zircon crystals. For example, two fragments of Group A zircon z11 exhibit distinct CA-TIMS dates that are outside of analytical uncertainty, a variation of ca. 10 ka. The trace element and TiZR data (Tables B.1 and B.2) support the two distinct ages; the LA-ICPMS analysis of the older fragment yields lower temperatures (ca. 790 °C) with higher REE concentrations while analysis of the younger fragment yields a higher temperature (ca. 810 °C) with lower REE concentrations. In this case, we interpret the LA-ICPMS and CA-TIMS analyses on fragment z11a as mixtures incorporating an internal core component of Group B zircon, while analyses of the z11b fragment capture the composition and age of the volumetrically dominant Group A rim.

These lines of evidence indicate that the new pulse of hot, more mafic ACR magma nucleated a small amount of new Group A zircon both homogeneously and heterogeneously on pre-existing Group B zircon. It should be emphasized that Group A forms a small proportion of the zircon population, consistent with inferences from Zr saturation and feldspar thermometry that the bulk ACR magma cooled only slightly below the Zr saturation temperature prior to eruption. The high aspect ratio of many Group A zircon grains is consistent with fast crystallization from a rapidly undercooled magma, perhaps in only locally Zr oversaturated domains or initially only on zircon antecrysts.

4.2. Implications for magma dynamics, crystal recycling, and zircon residence times

Several studies have proposed that hotter, more mafic melt was injected into other pre-existing silicic magmatic centers, based on similar variations in phenocryst composition and crystallization temperatures within a single eruptive unit (e.g. Campbell et al., 2009; Schmitt et al., 2003a, 2003b; Wark et al., 2007). A similar interpretation can be made in the case of the ACR system (Fig. 8). The combined geothermometry and geochemistry of the ACRz suggest that a hotter, less fractionated magma was injected into the Geysers–Cobb Mountain magmatic system at ca. 1.2 Ma. Although basaltic vents are not prevalent within the Geysers-Clear Lake Volcanic Field (Hearn et al., 1981), nearby nearly coeval basaltic vents exist (e.g. Caldwell Pines; Hammersley and DePaolo, 2006; Schmitt et al., 2006), as well as noritic to gabbroic xenoliths entrained in the mafic rocks that are evidence for mafic intrusives at depth (Stimac, 1993; Stimac et al., 1993). This is supported by geophysical evidence for small-bodied, mafic intrusions emplaced in the lower crust at depths of 12–24 km, with a northwesterly orientation (Stanley et al., 1998; Stimac et al., 2001). Cobb Mountain straddles one of these northwest-trending faults, which may have acted as the conduit for both intruding mafic magmas and the erupting rhyolite (Stimac et al., 2001). The abundance of older, low-T zircon antecrysts in the ACR also demands contributions to silicic magma generation from earlier crystallized, and subsequently remelted, plutons. Thus, the geological and geophysical data are consistent with zircon-based evidence for mafic recharge into the Geysers–Cobb Mountain magma system. This recharge was concomitant with partial remelting of earlier intrusives of the Geysers Plutonic Complex as recorded in Group B and rapid differentiation as recorded by Group A to produce rhyodacite to rhyolite eruptives including the ACR (Schmitt et al., 2003a).

The weighted mean CA-TIMS $^{206}Pb/^{238}U$ date for the youngest population among the Group A zircon of 1.1978 ± 0.0046 Ma is significantly younger than the peak of the zircon date distribution determined by IMP (Schmitt et al., 2003a). There are likely three factors for this difference: (1) the relatively minor abundance of Group A zircon, (2) their lower U content, and (3) the prevalence of interior spot analyses in sectioned crystals that bias against late-stage zircon rims. The first point is evidenced by the small number of Group A grains found in the UCLA mount; the much larger number of grains in the BSU mount were needed to identify both populations. Second, low U contents of Group A zircon would result in larger analytical uncertainties in IMP measurements, which would mask their significance. The higher U of Group B zircon yields more precise dates, which in turn would dominate any weighted mean calculations on a mixed population. Discerning the two populations was achieved by combining in situ geochemical criteria and greater analytical precision on individual measurements through the tandem LA-ICPMS and CA-TIMS approach.

Abundant geochemical and geochronological evidence links Group B zircon to earlier plutonic activity in the Geysers–Cobb Mountain magmatic system. Their abundance in the ACR, likely greater than 90% of the population, necessitates efficient crystal entrainment and recycling from earlier, solidified magma batches. This conclusion is in accord with the earlier inferences of Schmitt et al. (2003a, 2003b). While the evidence for some dissolution and overgrowth on entrained Group B crystals was previously discussed, the prismatic form of the vast majority of Group B zircon must also be explained. The generation of the ACR magma body via mafic injection and remelting of plutonics, and its subsequent extraction, rise, and eruption must have been relatively fast, with insufficient time for substantial dissolution of entrained zircon antecrysts within the undersaturated ACR magma.

Rapid timescales of ACR magma accumulation prior to eruption are directly supported by the small difference between the 1.1978 ± 0.0046 Ma mean differentiation age from Group A zircon and the eruptive $^{40}Ar/^{39}Ar$ ACRs age of 1.1850 ± 0.0016 Ma. This difference of 13 ± 5 ka places strong constraints on ACR storage times in the upper crust, and is consistent with numerical modeling of heat flow in the Geysers geothermal system (Norton and Hulen, 2001) and K-feldspar $^{40}Ar/^{39}Ar$ thermochronology of associated plutonic rocks (Dalrymple et al., 1999). In fact, the timescales of ACR differentiation may be even shorter if unrecognized Group B domains exist in the Group A zircon population, or if potential $^{230}Th/^{238}U$ disequilibrium of the ACR magma is considered. In the ^{230}Th disequilibrium correction of $^{206}Pb/^{238}U$, the initial magma $^{230}Th/^{238}U$ activity ratio is assumed to be unity, lacking any measured constraints for samples now at secular equilibrium. Actual magmatic $^{230}Th/^{238}U$

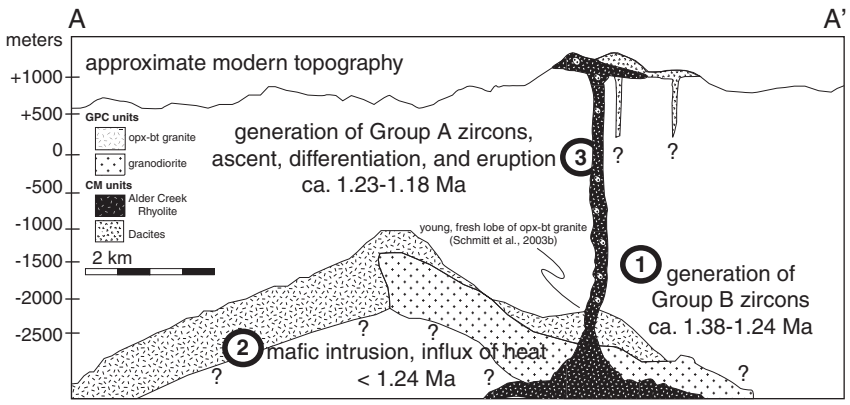

Fig. 8. Cartoon of magmatic events at Cobb Mountain and the Geyser Plutonic Complex (after Dalrymple et al., 1999). 1) crystallization of the main Geyser Plutonic Complex and Group B zircon crystals; 2) injection of mafic magma followed by ascent and differentiation of the ACR magma body with entrained lithic fragments of GPC rocks; 3) final ascent and eruption of ACR at 1.185 Ma. Approximate location of the cross section is given in Fig. 1.

activity ratios greater than unity, as often measured in Holocene to Pleistocene rhyolites (Jicha et al., 2007; Reagan et al., 2003; Lowenstern et al., 2006), will result in an overestimation of disequilibrium corrected $^{206}Pb/^{238}U$ ages by +4 ka per 5% ^{230}Th excess. Thus a plausible 5 to 10% ^{230}Th excess would yield a difference between ACR zircon and sanidine ages of only 8 to 4 ka. We conclude that in the case of the ACR-Geysers Plutonic Complex magma system, the truly magmatic "residence time" of crystals in the ACR magma was very short, numbering in the thousands of years prior to eruption, consistent with other residence time estimates for silicic magmas (e.g. Crowley et al., 2007). Previous inferences of crystal residence over hundreds of thousands of years (Simon et al., 2008) can largely be attributed to crystal recycling from the remelting of young plutonic wall-rocks (Schmitt et al., 2003a).

4.3. Implications for the ACRs $^{40}Ar/^{39}Ar$ age and the Cobb Mountain subchron

Our $^{40}Ar/^{39}Ar$ age for ACRs of 1.1850 ± 0.0016 Ma is calculated relative to the recently published astronomically calibrated value for FCs of 28.172 ± 0.028 Ma (Rivera et al., 2011). This is significantly younger than the widely used value of Nomade et al. (2005), particularly when that result is recalculated to the same FCs age (1.199 ± 0.002 Ma) or to an FCs age determined via intercalibration with U–Pb (1.2056 ± 0.0038 Ma; Renne et al., 2011), but is close to the mean value of the EARTHTIME intercalibration experiment involving 16 laboratories (Heizler and EARTHTIME Ar working group, 2008). Our value is also within uncertainty of the ACs-2 $^{40}Ar/^{39}Ar$ age obtained on the Stanford Noblesse (Coble et al., 2011), which used a different experimental approach to intercalibrate the detectors of their instrument than that used at the QUADLAB. Further, our ACRs age is supported by our CA-TIMS zircon study, where Group A zircon have a weighted mean $^{206}Pb/^{238}U$ age of 1.1978 ± 0.0046 Ma. The ca. 13 ka difference in $^{40}Ar/^{39}Ar$ sanidine and $^{206}Pb/^{238}U$ zircon ages can be accounted for by a short pre-eruptive residence interval for the zircon crystals, or by adjusting for ^{230}Th excess, which would then place the dates determined by the two techniques within uncertainty of each other. On the other hand, the recalculated $^{40}Ar/^{39}Ar$ age of Nomade et al. (2005) is *older* than the $^{206}Pb/^{238}U$ zircon age determined here. This reversal of U–Pb zircon and $^{40}Ar/^{39}Ar$ sanidine ages is geologically implausible, suggesting some source of bias in the calculated $^{40}Ar^*/^{39}Ar_K$ for ACRs of Nomade et al. (2005).

Since its initial recognition as a distinct geomagnetic polarity event (Mankinen et al., 1978), the Cobb Mountain subchron (C1r.2n) has been documented in deep sea drilling sites and recognized as a global event. Numerous ages have been proposed for the duration of the subchron based on a variety of age models from magnetostratigraphic and oxygen isotope records. Because the ACR is associated with the Cobb Mountain geomagnetic polarity subchron, we can compare radio-isotopic dating results for the extrusion of ACR to astronomical age estimates for the subchron.

Astronomical dating is a useful, independent alternative to radio-isotopic dating because it eliminates the dependence on neutron fluence monitors and the knowledge of an accurate and precise decay constant. Moreover, astronomical ages can provide an age for a geologic event, sample, or horizon nearing or achieving the ±0.1% EARTHTIME goal (e.g. Kuiper et al., 2008; Rivera et al., 2011). Regular fluctuations in the Earth's orbital parameters – precession (~21 ka cycle), obliquity (~41 ka cycle), and eccentricity (~100 and 405 ka, and 2.1 Ma cycles) – are precisely calculated as astronomical target curves based upon insolation variation over time (e.g. Laskar et al., 2004, 2011). The mix of the Earth's orbital cycles directly influence insolation, in turn affecting sedimentation type and rates or influencing the presence of certain types of benthic foraminifera within a marine sedimentary section. Logged cyclic variations preserved as proxy data in a sedimentary sequence, such as color or oxygen isotope values, for marine records can be correlated (tuned) to the calculated target curves, thus providing an astronomical age model for the sequence. Once a section is tuned, any event within that section can be assigned an astronomical age and uncertainty. For example, Plio–Pleistocene geomagnetic polarity reversals, including the Cobb Mountain subchron, preserved in globally distributed drill cores have been independently tuned and compiled into the most complete Geologic Time Scale (GTS2012; Gradstein et al., 2012).

Shackleton et al. (1990) provided an orbital-based age model for the Cobb Mountain subchron from ODP Site 677 (Equatorial Pacific) based on the correlation of the benthic and planktic oxygen isotope record to the Earth's precessional signal. They arrived at an age of 1.19 Ma using the Imbrie and Imbrie (1980) ice volume model, built upon the Berger and Loutre (1988) July 65° N insolation curve. Using this record as a reference core, Channell and Kleiven (2000) matched the benthic $\delta^{18}O$ record from ODP Site 983 (North Atlantic) to the same ice volume model, yet did not provide an estimate for the age of the subchron. This was followed by an expanded study of ODP Sites 983 and 984, where a band-pass filtered volume susceptibility record was matched to the precessional target curve of Berger and Loutre (1988). However, the age model for ODP Sites 983 and 984 cores was determined through matching the susceptibility record to the ODP Site 677 $\delta^{18}O$ record. From this analysis, an age of 1.190 to 1.215 Ma was assigned as the duration of the Cobb Mountain subchron (Channell et al., 2002).

A different approach to obtaining an astronomical age for the Cobb Mountain subchron by Horng et al. (2002) was based on records from the giant piston core MD972143 (Philippine Sea). Here, the band-pass

filtered $\delta^{18}O$ record was matched to the obliquity and precession target curves of the $La93_{(1,1)}$ astronomical solution (Laskar et al., 1993). Horng et al. (2002) highlight that the sedimentation record preserved in the core must be adjusted for the thicknesses of tephra deposits, and thus remove approximately 1 m of core to obtain a more realistic, continuous $\delta^{18}O$ record. Further, the authors account for orbital lag by adding 3 ka and 7 ka to the astronomical ages of precession and obliquity, respectively. Following these corrections, a duration of 1.173 ± 0.004 to 1.185 ± 0.005 Ma was proposed for the Cobb Mountain subchron. The errors were assigned based on uncertainties in the sedimentation rates and magnetostratigraphy, and do not include uncertainties associated with the astronomical solution itself.

We argue that the method employed by Horng et al. (2002) results in a more accurate astronomical age for the subchron, particularly in that it uses a more recent astronomical solution. Moreover, the peak-to-peak relationships between the filtered sample record and target curves are better correlated for the MD972143 core than for the ODP Site 983 and 984 records. Channell et al. (2002) note the mismatch between the filtered susceptibility record and astronomical target curves at Sites 983 and 984 and attribute the discrepancies to noise within the susceptibility record, possibly from the presence of volcanic ashes. Because of this mismatch and unknown lag times, Channell et al. (2002) refrained from "tuning the filtered susceptibility record to the astronomical solution." Therefore, the most convincing astronomical record to date for the age of the Cobb Mountain subchron is that of Horng et al. (2002), yet we advise a new tuning that utilizes the more recent astronomical solutions of Laskar et al. (2004, 2011).

The ACR $^{40}Ar/^{39}Ar$ sanidine eruption age obtained in this study supports the astronomical age determined by Horng et al. (2002). Oxygen isotope records of ODP Sites 983 and 984 and other North Atlantic locations were subsequently tuned by Channell et al. (2010) to an ice volume age model to evaluate the timing of the Matuyama–Brunhes polarity reversal. From this study, the authors calculated a best-fit age for FCs of 27.93 Ma, determined by aligning the age of Hawaiian basalts that preserve the reversal with the astronomical age of the boundary from the drill cores (Coe et al., 2004). Using this age for FCs in our experiments yields an ACRs age of 1.1748 ± 0.0007 Ma, distinguishably younger (up to ca. 0.04 Ma) than the astronomical age of the Cobb Mountain subchron from these same ODP cores (Channell and Kleiven, 2000; Channell et al., 2002). However, it should be noted that the new ice volume age model presented in Channell et al. (2010) does not extend to the Cobb Mountain subchron, and the astronomical age calculated here is only an estimate. The discrepancy between the astronomical age proposed for the subchron and that calculated using the monitor value that satisfies other boundaries within the same core might be resolved in the future when the ice volume tuning is extended. Therefore, at this time, the radio-isotopic ages suggest that the tuning of the MD972143 piston core studied by Horng et al. (2002) is the most accurate.

5. Conclusions

Contributions to the Quaternary geologic timescale via high-precision radio-isotopic anchors are essential to improving our understanding of geologic, climatic, and human events. The Cobb Mountain normal subchron is best represented by the ACR, which hosts the Quaternary $^{40}Ar/^{39}Ar$ mineral dating standard. In situ LA-ICPMS analyses combined with CA-TIMS $^{206}Pb/^{238}U$ dating of ACR zircon show trace element signatures representative of two distinct zircon populations: an older (1.38 to 1.24 Ma), low-temperature pre-eruptive suite that crystallized in a highly fractionated magma (Group B) and a younger (1.197 Ma), high-temperature eruptive suite (Group A) with a chemical composition indicative of a less fractionated magma. Group B zircon crystals are antecrysts scavenged from earlier intrusives of the Geysers Plutonic Complex, whereas Group A crystals reflect the injection and differentiation of the ACR magma body with heterogeneous nucleation of younger overgrowths on the Group B zircon antecrysts and rarer homogeneous nucleation of elongate prismatic crystals. The transition between the two groups at ca. 1.2 Ma is likely due to the influx of a less fractionated, mafic magma (possibly resembling the norites and gabbros found in the Clear Lake Volcanic Field) into the existing felsic magma system. The younger zircon crystals yield a weighted mean date of 1.1978 ± 0.0046 Ma that is slightly older than the eruptive $^{40}Ar/^{39}Ar$ single crystal sanidine age of 1.1850 ± 0.0016 Ma. The maximum zircon crystal residence time of <13 ka and preservation of antecrystic, pluton-derived zircons within the Zr undersaturated ACR magma is evidence for rapid generation, crystallization, and differentiation of the ACR magma batch. Our interpreted ACR eruption age of 1.1850 ± 0.0016 Ma is further supported by the astronomical age of the Cobb Mountain subchron based on the tuning of chemical proxy data to astronomical target curves, spanning from 1.185 ± 0.005 Ma to 1.173 ± 0.004 Ma (Horng et al., 2002). We, therefore, recommend the use of 1.1850 ± 0.0016 Ma as the age of the Quaternary mineral dating standard for future $^{40}Ar/^{39}Ar$ age experiments.

Supplementary data to this article can be found online at http://dx.doi.org/10.1016/j.chemgeo.2013.02.021.

Acknowledgments

This manuscript benefited from the contributions of L. Reisberg (editor), A. Schmitt, and an anonymous reviewer. A. Schmitt provided bulk rock and zircon samples, as well as essential comments that improved an earlier version of this manuscript. M. Heizler (New Mexico Institute of Technology) provided the purified separate of Fish Canyon sanidine. K. Kuiper (Vjire University Amsterdam, Utrecht University) provided the A1Ts separate. We thank D. Pierce and M. Hill for technical assistance (BSU), P. Olin for LA-ICPMS assistance (BSU), C. Zeeden for assistance with astronomical solutions (UU), and the EARTHTIME and GTSnext communities for useful discussions. The research leading to these results has received funding from the European Community's Seventh Framework Programme (FP7/2007–2013) under grant agreement no. 215458. The Quaternary Dating Laboratory, hosted at Roskilde University, is funded by the Villum Foundation.

References

Berger, A., Loutre, M.F., 1988. New insolation values for the climate of the last 10 million years. Sci. Rep. 1988/13.Institut d'Astronomie et de Geophysique Georges Lemaitre. Universite Catholique de Louvain-la-Neuve.

Bindeman, I.N., Valley, J.M., Wooden, J.L., Persing, H.M., 2001. Post-caldera volcanism: in situ measurement of U–Pb age and oxygen isotope ratio in Pleistocene zircons from Yellowstone caldera. Earth and Planetary Science Letters 189, 197–206.

Brumm, A., Jensen, G.M., van den Bergh, G.D., Morwood, M.J., Kurniawan, I., Aziz, F., Storey, M., 2010. Hominins on Flores, Indonesia, by one million years ago. Nature 464, 748–752.

Campbell, M.E., Hanson, J.B., Minarik, W.G., Stix, J., 2009. Thermal history of the Bandelier magmatic system: evidence for magmatic injection and recharge at 1.61 Ma as revealed by cathodoluminescence and titanium geothermometry. Journal of Geology 117, 469–485.

Channell, J.E.T., Kleiven, H.F., 2000. Geomagnetic palaeointensities and astrochronological ages for the Matuyama–Brunhes boundary and the boundaries of the Jaramillo Subchron: palaeomagnetic and oxygen isotope records from ODP Site 983. Philosophical Transactions of the Royal Society of London 358, 1027–1047.

Channell, J.E.T., Mazaud, A., Sullivan, P., Turner, S., Raymo, M.E., 2002. Geomagnetic excursions and paleointensities in the Matuyama Chron at Ocean Drilling Program Sites 983 and 984 (Iceland Basin). Journal of Geophysical Research 107, 2114.

Channell, J.E.T., Hodell, D.A., Singer, B.S., Xuan, C., 2010. Reconciling astrochronological and $^{40}Ar/^{39}Ar$ ages for the Matuyama–Brunhes boundary and late Matuyama Chron. Geochemistry, Geophysics, Geosystems 11, Q0AA12.

Coble, M.A., Grove, M., Calvert, A.T., 2011. Calibration of Nu-Instruments Noblesse multicollector mass spectrometers for argon isotopic measurements using a newly developed reference gas. Chemical Geology 290, 75–87.

Coe, R.S., Singer, B.S., Pringle, M.S., Zhao, X., 2004. Matuyama–Brunhes reversal and Kamikatsura event on Maui: paleomagnetic directions, $^{40}Ar/^{39}Ar$ ages and implications. Earth and Planetary Science Letters 222, 667–684.

Condon, D., Schoene, B., Bowring, S.A., Parrish, R., McLean, N., Noble, S., Crowley, Q., 2007. EARTHTIME: isotopic tracers and optimized solutions for high-precision U–Pb ID-

TIMS geochronology. EOS. Transactions of the American Geophysical Union 88 (52) (abs. V41E-06).
Crowley, J.L., Schoene, B., Bowring, S.A., 2007. U-Pb dating of zircon in the Bishop Tuff at the millennial scale. Geology 35, 1123–1126. http://dx.doi.org/10.1130/G24017A.1.
Dalrymple, G.B., Grove, M., Lovera, O.M., Harrison, T.M., Hulen, J.B., Lanphere, M.A., 1999. Age and thermal history of the Geysers plutonic complex (felsite unit), Geysers geothermal field, California; a $^{40}Ar/^{39}Ar$ and U–Pb study. Earth and Planetary Science Letters 30, 285–298.
Davydov, V.I., Crowley, J.L., Schmitz, M.D., Poletaev, V.I., 2010. High-precision U–Pb zircon age calibration of the global Carboniferous time scale and Milankovitch band cyclicity in the Donets Basin, eastern Ukraine. Geochemistry, Geophysics, Geosystems 11, Q0AA04.
Donnelly-Nolan, J.M., Burns, M.G., Goff, F.E., Peters, E.K., Thompson, J.M., 1993. The Geysers-Clear Lake area, California: thermal waters, mineralization, volcanism, and geothermal potential. Economic Geology 88, 301–316.
EARTHTIME website, d. www.earth-time.org (Accessed September 5, 2012).
Ferry, J.M., Watson, E.B., 2007. New thermodynamic models and revised calibrations for the Ti-in-zircon and Zr-in-rutile thermometers. Contributions to Mineralogy and Petrology 154, 429–437.
Gradstein, F.M., Ogg, J.G., Schmitz, M.D., Ogg, G.M., 2012. The Geologic Time Scale 2012. Elsevier, San Francisco, CA.
Hammersley, L., DePaolo, D.J., 2006. Isotopic and geophysical constraints on the structure and evolution of the Clear Lake volcanic system. Journal of Volcanology and Geothermal Research 153, 331–356.
Hayden, L.A., Watson, E.B., 2007. Rutile saturation in hydrous siliceous melts and its bearing on Ti-thermometry of quartz and zircon. Earth and Planetary Science Letters 258, 561–568.
Hearn Jr., B.C., Donnelly-Nolan, J.M., Goff, F., 1981. The Clear Lake Volcanics; tectonic setting and magma sources. U.S. Geol. Surv. Prof. Paper 1141, No. 25–4.
Heizler, M.T., EARTHTIME Ar working group, 2008. Argon Laboratory Intercomparison Efforts for the EARTHTIME Initiative (EGU2008-A-11478; SSP10, Vienna, Austria).
Hilgen, F.J., Krijgsman, W., Langereis, C.G., Lourens, L.J., Santarelli, A., Zachariasse, W.J., 1995. Extending the astronomical (polarity) time scale in the Miocene. Earth and Planetary Science Letters 136, 495–510.
Hinton, R.W., Upton, B.G.J., 1991. The chemistry of zircon: variations within and between large crystals from syenite and alkali basalt xenoliths. Geochimica et Cosmochimica Acta 55, 3287–3302.
Horng, C.-S., Lee, M.-Y., Palike, H., Wei, K.-Y., Liand, W.-T., Iizuka, Y., Torii, M., 2002. Astronomically calibrated ages for geomagnetic reversals within the Matuyama chron. Earth Planets Space 54, 679–690.
Hoskin, P.W.O., Ireland, T.R., 2000. Rare earth element chemistry of zircon and its use as a provenance indicator. Geology 28, 627–630.
Hulen, J.B., Nielson, D.L., 1993. Interim report on geology of the Geysers felsite, Northwestern California. Geothermal Resources Council Transactions 17, 249–258.
Imbrie, J., Imbrie, J.Z., 1980. Modeling the climatic response to orbital variations. Science 207, 943–953.
Jaffey, A.H., Flynn, K.F., Glendenin, L.E., Bentley, W.C., Essling, A.M., 1971. Precision measurement of half-lives and specific activities of ^{235}U and ^{238}U. Physics Review C4, 1889–1906.
Jicha, B.R., Singer, B.S., Beard, B.L., Johnson, C.M., Moreno-Roa, H., Naranjo, J.A., 2007. Rapid magma ascent and generation of ^{230}Th excesses in the lower crust at Puyehue-Cordón Caulle, Southern Volcanic Zone, Chile. Earth and Planetary Science Letters 255, 229–242.
Kuiper, K.F., Hilgen, F.J., Steenbrink, J., Wijbrans, J.R., 2004. $^{40}Ar/^{39}Ar$ ages of tephras intercalated in astronomically tuned Neogene sedimentary sequences in the eastern Mediterranean. Earth and Planetary Science Letters 222, 583–597.
Kuiper, K.F., Deino, A., Hilgen, F.J., Krijgsman, W., Renne, P.R., Wijbrans, J.R., 2008. Synchronizing rock clocks of Earth history. Science 320, 500–504.
Laskar, J., Joutel, F., Boudin, F., 1993. Orbital, precessional, and insolation quantities for the Earth from −20 Myr to +10 Myr. Astronomy and Astrophysics 270, 522–533.
Laskar, J., Robutel, P., Joutel, F., Gastineau, M., Correia, A.C.M., Levrard, B., 2004. A long-term numerical solution for the insolation quantities of the Earth. Astronomy and Astrophysics 428, 261–265.
Laskar, J., Fienga, A., Gastineau, M., Manche, H., 2011. La2010: a new orbital solution for the long-term motion of the Earth. Astronomy and Astrophysics 532.
Lee, J.-Y., Marti, K., Severinghaus, J.P., Kawamura, K., Yoo, H.-S., Lee, J.B., Kim, J.S., 2006. A redetermination of the isotopic abundances of atmospheric Ar. Geochimica et Cosmochimica Acta 70, 6.
Lowenstern, J.B., Charlier, B.L.A., Clynne, M.A., Wooden, J.L., 2006. Extreme U–Th disequilibrium in rift-related basalts, rhyolites, and granophyric granite and the timescales of rhyolite generation, intrusion and crystallization at Alid Volcanic Center, Eritrea. Journal of Petrology 47, 2105–2112.
Mankinen, E.A., Donnelly, J.M., Gromme, C.S., 1978. Geomagnetic polarity event recorded at 1.1 m.y. B.P. on Cobb Mountain, Clear Lake volcanic field, California. Geology 6, 653–656.
Mattinson, J.M., 2005. Zircon U–Pb chemical abrasion ("CA-TIMS") method: combined annealing and multi-step partial dissolution analysis for improved precision and accuracy of zircon ages. Chemical Geology 220, 47–66.
Meyers, S.R., Siewert, S.E., Singer, B.S., Sageman, B.B., Condon, D.J., Obradovich, J.D., Jicha, B.R., Sawyer, D.A., 2012. Intercalibration of radioisotopic and astrochronologic time scales for the Cenomanian–Turonian boundary interval, Western Interior Basin, USA. Geology 40, 7–10.
Min, K., Mundil, R., Renne, P.R., Ludwig, K.R., 2000. A test for systematic errors in $^{40}Ar/^{39}Ar$ geochronology through comparison with U/Pb analysis of a 1.1-Ga rhyolite. Geochimica et Cosmochimica Acta 64, 73–98.
Nomade, S., Renne, P.R., Vogel, N., Deino, A.L., Sharp, W.D., Becker, T.A., Jaouni, A.R., Mundil, R., 2005. Alder Creek sanidine (ACs-2): a Quaternary $^{40}Ar/^{39}Ar$ dating standard tied to the Cobb Mountain geomagnetic event. Chemical Geology 218, 315–338.
Norton, D.L., Hulen, J.B., 2001. Preliminary numerical analysis of the magma-hydrothermal history of the Geysers geothermal system, California, USA. Geothermics 30, 211–234.
Powell, R., Hergt, J., Woodhead, J., 2002. Improving isochron calculations with robust statistics and the bootstrap. Chemical Geology 185, 191–204.
Reagan, M.K., Sims, K.W.W., Erich, J., Thomas, R.B., Cheng, H., Edwards, R.L., Layne, G., Ball, L., 2003. Time-scales of differentiation from mafic parents to rhyolite in North American continental arcs. Journal of Petrology 144, 1703–1726.
Reid, M.R., Coath, C.D., Harrison, T.M., McKeegan, K.D., 1997. Prolonged residence times for the youngest rhyolites associated with Long Valley Caldera; $^{230}Th–^{238}U$ ion microprobe dating of young zircons. Earth and Planetary Science Letters 150, 27–39.
Reid, M., Vazquez, J., Schmitt, A., 2011. Zircon-scale insights into the history of a supervolcano, Bishop Tuff, Long Valley, California, with implications for the Ti-in-zircon geothermometer. Contributions to Mineralogy and Petrology 161, 293–311.
Renne, P.R., Balco, G., Ludwig, K.R., Mundil, R., Min, K., 2011. Response to the comment by W.H. Schwarz et al. on "Joint determination of ^{40}K decay constants and $^{40}Ar^*/^{40}K$ for the Fish Canyon sanidine standard, and improved accuracy for $^{40}Ar/^{39}Ar$ geochronology" by P.R. Renne et al. (2010). Geochimica et Cosmochimica Acta 75, 5097–5100.
Rivera, T.A., Storey, M., Zeeden, C., Hilgen, F.J., Kuiper, K., 2011. A refined astronomically calibrated $^{40}Ar/^{39}Ar$ age for Fish Canyon sanidine. Earth and Planetary Science Letters 311, 420–426.
Rubatto, D., 2002. Zircon trace element geochemistry: partitioning with garnet and the link between U–Pb ages and metamorphism. Chemical Geology 184, 123–138.
Schmitt, A.K., 2011. Uranium series accessory dating of magmatic processes. Annu. Rev. Earth Planet. Sci. 39, 321–349.
Schmitt, A.K., Grove, M., Harrison, T.M., Lovera, O., Hulen, J., Walters, M., 2003a. The Geysers–Cobb Mountain Magma System, California (Part I): U–Pb zircon ages of volcanic rocks, conditions of zircon crystallization and magma residence times. Geochimica et Cosmochimica Acta 67, 3423–3442.
Schmitt, A.K., Grove, M., Harrison, T.M., Lovera, O., Hulen, J., Walters, M., 2003b. The Geysers–Cobb Mountain Magma System, California (Part 2): timescales of pluton emplacement and implications for its thermal history. Geochimica et Cosmochimica Acta 67, 3443–3458.
Schmitt, A.K., Romer, R., Stimac, J.A., 2006. Geochemistry of volcanic rocks from the Geysers geothermal area, California Coast Ranges. Lithos 87, 80–103.
Schmitz, M.D., Schoene, B., 2007. Derivation of isotope ratios, errors, and error correlations for U–Pb geochronology using $^{205}Pb–^{235}U–(^{233}U)$-spiked isotope dilution thermal ionization mass spectrometric data. Geochemistry, Geophysics, Geosystems 8, Q08006.
Schoene, B., Crowley, J.L., Condon, D.J., Schmitz, M.D., Bowring, S.A., 2006. Reassessing the uranium decay constants from geochronology using ID-TIMS U–Pb data. Geochimica et Cosmochimica Acta 70, 426–445.
Shackleton, N.J., Berger, A., Peltier, W.R., 1990. An alternative astronomical calibration of the lower Pleistocene timescale based on ODP Site 677. Transactions of the Royal Society of Edinburgh: Earth Sciences 81, 251–261.
Simon, J.I., Renne, P.R., Mundil, R., 2008. Implications of pre-eruptive magmatic histories of zircons for U–Pb geochronology of silicic extrusions. Earth and Planetary Science Letters 266, 182–194.
Smith, M.E., Chamberlain, K.R., Singer, B.S., Carroll, A.R., 2010. Eocene clocks agree: coeval $^{40}Ar/^{39}Ar$, U–Pb, and astronomical ages from the Green River Formation. Geology 38, 527–530.
Stanley, W.D., Benz, H.M., Walters, M.A., Villaseñor, A., Rodriguez, B.D., 1998. Tectonic controls on magmatism in the Geysers-Clear Lake region: evidence from new geophysical models. Geological Society of America Bulletin 110, 1193–1207.
Stimac, J.A., 1993. Origin and significance of high-grade metamorphic xenoliths, Clear Lake, California. In: Rytuba, J.J. (Ed.), Active Geothermal Systems and Gold–Mercury Deposits in the Sonoma-Clear Lake Volcanic Fields, California: Society of Economic Geologists Guidebook Series, 16, pp. 171–189.
Stimac, J.A., Donnelly-Nolan, J.D., Bullen, T., McLaughlin, R., Jacobs, D., Smith, B., 1993. Isotopic evidence for open-system magmatism at Clear Lake, California. International Association of Volcanology and Chemistry of the Earth's Interior General Assembly, Canberra Australia, p. 107.
Stimac, J.A., Goff, F., Wohletz, K., 2001. Thermal modeling of the Clear Lake magmatic–hydrothermal system, California, USA. Geothermics 30, 349–390.
Storey, M., Duncan, R.A., Swisher, C.C., 2007. Paleocene–Eocene thermal maximum and the opening of the Northeast Atlantic. Science 316, 587–589.
Storey, M., Roberts, R.G., Saidin, M., 2012. Astronomically calibrated $^{40}Ar/^{39}Ar$ age for the Toba supereruption and global synchronization of late Quaternary records. Proceedings of the National Academy of Science 109, 18684–18688.
Trail, D., Watson, E.B., Tailby, N.D., 2012. Ce and Eu anomalies in zircon as proxies for the oxidation state of magmas. Geochimica et Cosmochimica Acta 97, 70–87.
Turrin, B.D., Donnelly-Nolan, J.M., Hearn Jr., B.C., 1994. $^{40}Ar/^{39}Ar$ ages from the rhyolite of Alder Creek, California: age of the Cobb Mountain Normal-Polarity Subchron revisited. Geology 22, 251–254.
Wark, D.A., Hildreth, W., Spear, F.S., Cherniak, D.J., Watson, E.B., 2007. Pre-eruption recharge of the Bishop magma system. Geology 35, 235–238.
Watson, E.B., Harrison, T.M., 2005. Zircon thermometer reveals minimum melting conditions on earliest Earth. Science 308, 841–844.
Watson, E.B., Wark, D., Thomas, J., 2006. Crystallization thermometers for zircon and rutile. Contributions to Mineralogy and Petrology 151, 413–433.